IX International Conference on Computational Methods for Coupled Problems in Science and Engineering
COUPLED PROBLEMS 2021
E. Oñate, M. Papadrakakis and B. Schrefler (Eds)

MULTI-PHYSICS SIMULATIONS OF A WIND TURBINE IN ICING CONDITIONS

Francesco Caccia*†, Valentina Motta†† and Alberto Guardone†

Politecnico di Milano
Via La Masa 34, 20156 Milan, Italy
e-mail: francescoangelo.caccia@mail.polimi.it
alberto.guardone@polimi.it

†† GE Renewable Energy – Wind
Franklinstrasse 9-15a, Hofe building, 10587 Berlin, Germany
e-mail: valentina.motta@ge.com

Key words: Wind Turbine, Atmospheric Icing, Ice Accretion, Power Losses, CFD

Abstract. Wind turbines in cold climates are likely to suffer from icing events, deteriorating the aerodynamic performances of the blades and decreasing their power output. In this work, a 3-hour rime ice accretion event is numerically simulated on five significant sections of a wind turbine blade operating in steady wind using a high-fidelity procedure based on the Blade Element Momentum Theory. The onshore NREL 5MW reference wind turbine is studied. Ice accretion is simulated through a fine multi-step process, adding ice layers approximately 0.5 mm thick; each step consists of the successive coupling of a CFD simulation, a Lagrangian particle-tracking of the cloud droplets, an ice accretion step, and re-meshing of the new geometry. Ice roughness is modelled with an equivalent sand-grain approach. After computing the aerodynamic coefficients of ice-contaminated airfoils, power losses are obtained considering the aeroelastic response of the wind turbine in turbulent winds as defined by the Design Load Case 1.1. The effect of the extension of roughness on the surface of the blade is also assessed. In the considered operating conditions and accretion times, a strong dependence between the decrease in power output and the tip-speed ratio and a small dependence on surface roughness are found.

1 INTRODUCTION

In 2020, 16% of electricity demand in Europe was supplied by wind energy. Ambitious targets have been set to reach carbon neutrality by 2050: the share of wind energy in the total energy mix is expected to grow up to 30% by 2030 and at least to 50% by 2050. This goal will be reached by focusing investments on offshore wind and cold regions since these areas contain a higher wind power density, due to higher wind speeds and air density.

However, in cold regions ice may accrete on wind turbines when temperatures drop below 0 °C and clouds or super-cooled fog arise at low elevations. As ice is accreted on a blade, the change in shape of its sections deteriorates the aerodynamic performances of the airfoils, leading to a decrease in power extraction. Different numerical studies present in literature, all focusing on rime ice accretion in operating conditions, do not show a clear trend on power losses. Homola [1] simulated a 1 h icing event on the NREL 5 MW wind turbine [2], finding a power loss of approximately 25% between $7\,\mathrm{m\,s^{-1}}$ and $11\,\mathrm{m\,s^{-1}}$. Turkia [3], after 3 h, found a decrease in power extraction of approximately 25%, on a down-scaled version of the NREL 5 MW. Finally, the power loss found by Etemaddar [4] on the 5 MW wind turbine decreases from 34% to 23% in the same range of wind speeds, after a 24 h icing event; in this case, the power curve was generated in turbulent winds. Despite the different atmospheric conditions analysed, the main responsible for such incoherence in the results found may be ascribed to roughness modelling in CFD simulations: in fact, while Etemaddar applied surface roughness on the leading edge of the iced sections for $\frac{x}{c} < 25\%$, considering an equivalent sand-grain roughness height $\frac{k_s}{c} = 0.5 \cdot 10^{-3}$, Homola applied it to the whole blade ($\frac{k_s}{c}$ is not declared); Turkia, on the other hand, applied Bragg relations [5] to the drag coefficient of the iced sections, considering $\frac{k_s}{c} = 1 \cdot 10^{-3}$ (such relations, however, should be applied to the drag coefficient of a clean airfoil).

Given the above, the goal of the present contribution is to perform a high fidelity ice accretion simulation on the NREL 5 MW wind turbine blade to assess power losses after the icing event considering the atmospheric conditions shown in Table 1, i.e., the same analysed by Homola [1] and Zanon [6], for a total time of 180 min. Power curves are generated considering the atmospheric turbulence defined by the International Electrotechnical Commission (IEC) for the Dynamic Load Case (DLC) 1.1 [7]. The effect of the extension of roughness on the surface of the blade for the current icing event is also analysed.

The present paper is structured as follows. In Section 2, the methodology applied within this work is shown; in particular, Sections 2.1 and 2.2 contain details about the numerical setup of CFD and ice accretion simulations, respectively. Results are shown in Section 3, with ice accretion simulations in Section 3.1 and wind turbine performances before and after icing in Section 3.2. Conclusions are provided in Section 4.

Table 1: Atmospheric conditions in the icing event studied.

Duration [min]	V_∞ [$\mathrm{m\,s^{-1}}$]	Wind Shear Exponent	P_∞ [Pa]	ρ_{air} [$\mathrm{kg\,m^{-3}}$]	T_∞ [°C]	LWC [$\mathrm{g\,m^{-3}}$]	MVD [µm]
180	10	0.15	101325	1.341	-10	0.22	20

2 METHODOLOGY

The aerodynamics of the wind turbine is modelled through the Blade Element Momentum Theory (BEMT). The analysis is performed following the steps outlined below:

1. Firstly, clean airfoil data is reproduced for comparison with experimental results by solving Reynolds-Averaged Navier-Stokes (RANS) equations through an open-source CFD code, SU2 [8]. Details on the airfoils composing the outer half of the blade and the Reynolds number of the experimental data are provided in Table 2.

2. The aeroelastic response of the operating wind turbine is now simulated in the atmospheric conditions shown in Table 1 with OpenFAST [9]; a steady wind is assumed at this stage. After the simulation, local boundary conditions are evaluated on significant blade sections and used as input for ice accretion. A multi-step approach is adopted, dividing the total accretion time in sub-intervals. Each step consists in the successive coupling of a RANS simulation, a Lagrangian particle-tracking of the cloud droplets, an ice accretion step, and re-meshing of the new geometry, performed with SU2, PoliDrop [10], PoliMIce [11], and uhMesh [12], respectively. These codes are partly or entirely developed within Politecnico di Milano.

3. The aerodynamic coefficients of the iced sections are retrieved with SU2. The effect of roughness is taken into account, estimating the equivalent sand-grain roughness height using an empirical correlation by Wright [13], setting $\frac{k_s}{c} = 0.34 \cdot 10^{-3}$. Two cases are considered: in the first case, roughness is applied only where ice is predicted; in the second one, roughness is extended on the airfoil surface.

4. Finally, the power curve of the wind turbine is computed with OpenFAST, considering the atmospheric turbulence defined by the IEC for the DLC 1.1 of a Category B wind turbine. Power losses are estimated at the different wind speeds.

Table 2: Airfoils composing the outer half of the NREL 5 MW wind turbine blade.

Airfoil	Identifier	Radial position [%]	t/c [%]	Re [$-$]
DU 91-W2-250LM	DU25	$44.7 < r/R < 51.2$	25.0	$7 \cdot 10^6$
DU 93-W-210LM	DU21	$57.7 < r/R < 64.2$	21.0	$7 \cdot 10^6$
NACA 64_3-618	NA18	$70.7 < r/R < 100$	18.0	$6 \cdot 10^6$

2.1 Numerical Setup and Grid Convergence

The SU2 code solves RANS equations using an edge-based finite volume discretization in space. The convective and viscous fluxes are then evaluated at the midpoint of an edge. An upwind Flux Difference Splitting (FDS) numerical scheme is used to solve the convective fluxes; second-order accuracy of the numerical method is obtained by applying a MUSCL scheme for fluxes reconstruction. Green-Gauss theorem is used to evaluate the gradients of variables at each node. During reconstruction, gradients are limited with Venkatakrishnan slope limiter [14] to avoid spurious oscillations in the solution.

Simulations are considered at convergence when (a) the root mean square of the residual in the entire domain is reduced at least of three orders of magnitude for all variables, and (b) the normalized relative difference between two consecutive iterations of lift and drag coefficients, C_L and C_D, respectively, averaged over 100 iterations, is smaller than 10^{-6}.

2D hybrid grids are generated with uhMesh. The circular domain is made of a structured O-grid around the airfoil, required to resolve the boundary layer, surrounded by and an unstructured grid of triangular elements. A farfield radius of 240 chords (c) is chosen to ensure the independence of the solution from the domain dimension, while a first cell height of $10^{-6}c$ guarantees $y^+_{wall} < 1$ along the entire airfoil surface in all simulations. Three sets of grids are generated for each airfoil, doubling each time the dimension of the elements, to evaluate the uncertainty of the solution due to discretization error using the Grid Convergence Index (GCI) method [15]. The finest grid consists of approx. 150'000 elements, with characteristic lengths of $8c$ at the farfield, $\frac{0.3}{1000}c$ on the leading edge, $\frac{1}{1000}c$ on the trailing edge, and $\frac{10}{1000}c$ on the upper and lower surfaces. The GCI method is applied to fully-turbulent simulations using Spalart-Allmaras [16] turbulence model (SA) for RANS equations closure.

Once the accuracy of the finest grid is verified, simulations are repeated on this grid applying the algebraic Cakmakcioglu and Bas [17] transition model (SA-BC) with a freestream turbulence intensity of 0.1%. Lift and drag coefficients of the airfoils belonging to the outer half of the blade are shown in Figure 1, compared to the data provided by NREL prior to corrections for 3D effects. The discretization error computed with the GCI method, shown through an error bar, is sufficiently small in all simulations. By applying the transition model, excellent agreement is found with the experimental data, in particular with attached flows. As the flow detaches, an overestimation of the lift coefficient is found, which is more pronounced when the transition model is present. Such behaviour is normal and could be avoided through a re-calibration of the turbulence model.

On the iced airfoils, the effect of roughness on the boundary layer is modelled by applying the Boeing extension for Spalart-Allmaras turbulence model [18]. Ice shapes are finely discretized, fixing an element length of $\frac{c}{1000}$ where the presence of ice is predicted.

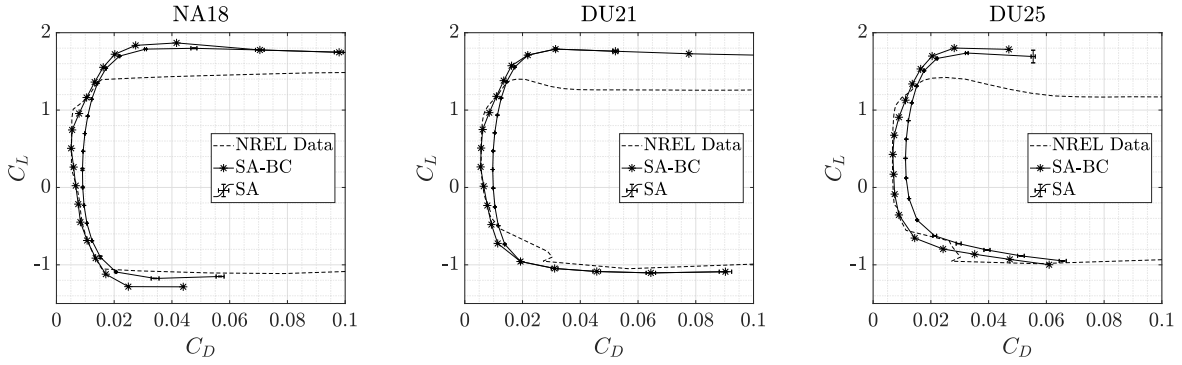

Figure 1: Drag polars of the airfoils belonging to the outer half of the blade.

2.2 Setup for Ice Accretion Simulations

Icing is monitored on five independent sections, belonging to the outer half of the blade, as shown in Figure 2. In particular, each section is located halfway between two nodes used for the computation of aerodynamic loads on the blade in the aeroelastic simulations; then, aerodynamic coefficients of the iced sections will be applied to the two adjacent nodes. Boundary conditions on each section are obtained by computing first the mean value of the periodic aeroelastic response of the wind turbine operating in steady wind on each node, and then the mean value between the two adjacent nodes. Over a blade revolution, the maximum deviation from the mean value of the angle of attack (AoA) and the relative velocity (V_{rel}) are 0.6° and $1\,\mathrm{m\,s^{-1}}$, respectively, and both can be neglected during ice accretion; a sensitivity analysis on these parameters is provided by Etemaddar [4]. The result of this process is shown in Table 3.

Table 3: Local boundary conditions on the five sections under analysis.

Section	Airfoil ID	r/R [−]	chord [m]	V_{rel} [$\mathrm{m\,s^{-1}}$]	AoA [deg]	Δt [min]
A	NA18	0.93	1.753	72.75	3.80	1
B	NA18	0.84	2.416	65.95	3.96	2
C	NA18	0.72	2.887	56.71	3.85	3
D	DU21	0.59	3.379	47.08	3.68	6
E	DU25	0.46	3.878	37.51	4.26	15

Within the multi-step ice accretion, a different time-step is used on each section. In fact, as the local velocity increases and chord and relative thickness decrease, i.e. towards the tip of the blade, the ice accretion rate increases [4], while it is desirable to add the same ice thickness in each accretion step to maintain the same level of accuracy on the different sections. Moreover, by adding a small ice thickness during each time-step, a

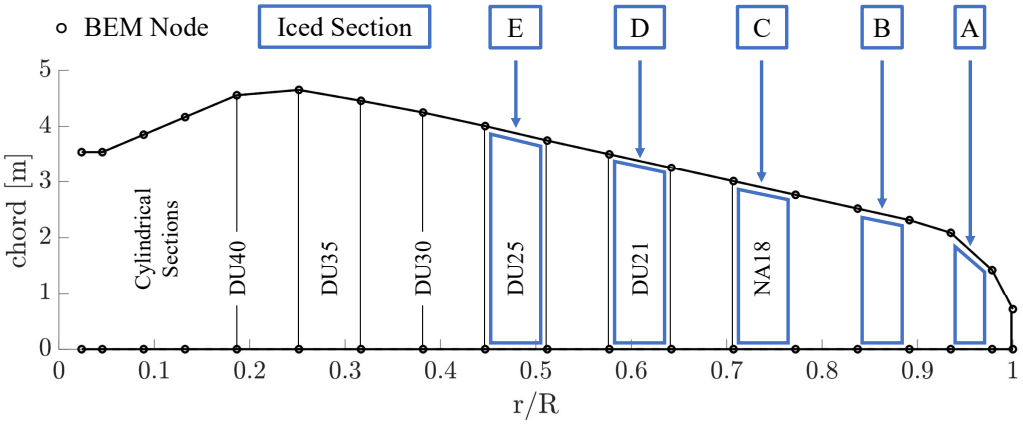

Figure 2: Blade discretization and sections monitored for icing.

better representation of the physics of the problem is provided by continuously updating the flow field due to the presence of ice, and by computing the collection efficiency (β) and accreting ice on the actual geometry. However, such an approach can easily become too computationally expensive. It is possible to save CPU time by increasing the residual in the computation of β: in fact, a large number of droplets must be used to obtain high accuracy. This does not affect the accuracy of the solution, since error propagation is highly reduced by accreting a small ice thickness during each step.

The validity of this approach is tested by comparing numerical results with experimental ice accretion on a rotating blade section, consisting of an S809 airfoil with $c = 0.267\,\mathrm{m}$, carried out by Han [19] in The Adverse Environment Rotor Test Stand (AERTS) of the Pennsylvania State University. AERTS test cases 20, 21 and 22 were chosen, since test conditions are similar to those of the icing event under analysis, as reported in Table 4. These test cases only differ in the duration of the icing event. Two approaches were tested, which are almost equal in terms of computational time. Results are compared in Figure 3: in the first approach, (a), the residual of β in PoliDrop is set to $3 \cdot 10^{-6}$, using a time-step of 15 min in PoliMIce; in the second one, (b), proposed in the current work, the residual is set to $3 \cdot 10^{-5}$, using a time-step of 3 min for ice accretion. While in both cases the impinged area on the lower surface is smaller with respect to the experimental results, it is clear that the ice shapes obtained on the leading edge using more time-steps are more accurate, despite the higher residual used for the computation of β. Moreover, the total elapsed time for the 90 min ice accretion is 7.5 h for approach (a), and 6.5 h for approach (b), being the latter 13% faster. For this reason, approach (b) is adopted, consisting in smaller time-steps and a residual on β of $3 \cdot 10^{-5}$.

Table 4: Test conditions of AERTS test cases 20-22.

Case #	MVD [µm]	LWC [g m^{-3}]	T [°C]	V_{rel} [m s^{-1}]	AoA [deg]	Time [min]
20 - 22	20.0	0.05	-9.0	50.0	4.0	30; 60; 90

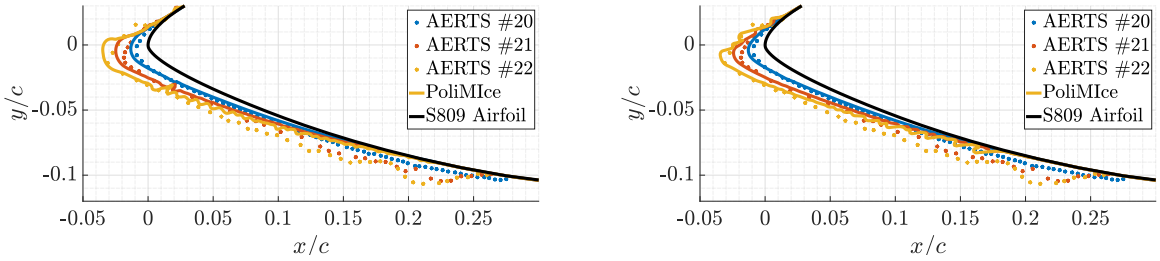

(a) $\Delta t = 15\,\mathrm{min}$; $\mathrm{res}(\beta) = 3 \cdot 10^{-6}$ **(b)** $\Delta t = 3\,\mathrm{min}$; $\mathrm{res}(\beta) = 3 \cdot 10^{-5}$

Figure 3: Comparison of numerical simulations with AERTS test cases 20-22.

3 RESULTS AND DISCUSSION

3.1 Ice Accretion and Aerodynamic Coefficients

Results of the ice accretion simulations on the blade are shown in Figure 4. It is worth noticing that during the simulations it was not necessary to update the boundary conditions: this was checked by applying an empirical correlation obtained through a sensitivity analysis in OpenFAST, estimating the variation of the angle of attack due to the variation in C_L and C_D. After the icing event, the increase of the AoA on all sections is smaller than 0.5°, while the relative velocity decreases of less than $3\,\mathrm{m\,s^{-1}}$.

The ice mass accreted on the blade increases almost linearly, from $0.42\,\mathrm{kg\,m^{-1}}$ on Section E to $3.35\,\mathrm{kg\,m^{-1}}$ on section A. The total accreted mass is estimated to be lower than 100 kg, i.e. less than 0.5% of the total blade mass, and may be neglected.

To assess the effect of the extension of roughness over the blade, the aerodynamic coefficients are computed in two cases: by applying roughness exclusively where the presence of ice is predicted (it will be denoted as *normal roughness*), and by extending its application for a length corresponding to 25% of the chord of Section A, i.e. 0.44m, on all sections, on both the upper and the lower surface (it will be denoted as *extended roughness*).

Results for normal roughness are shown in Figures 5 and 6: the degradation in performance for all aerodynamic coefficients increases as we move towards the outer sections. On all NACA sections, flow is completely detached from the lower surface already at −8°. Due to the small amount of ice accreted, for attached flows sections D and E behave similarly to their clean counterpart when flow transition is not considered, while stall is still slightly anticipated.

The percentage variation in the aerodynamic coefficients for the case of extended roughness, with respect to the normal one, is shown in Figure 7. Results for $\alpha = -4°$, which is very close to the zero-lift angle, have been omitted. For NACA sections, considering attached flows, Section A is the most sensitive: in fact, the ice shape is already well developed on all three sections, but Section A has the smallest chord. On the other hand, for DU sections, Section E suffers the extension of roughness more than Section D, since, despite the longer chord, almost no ice was accreted on this section.

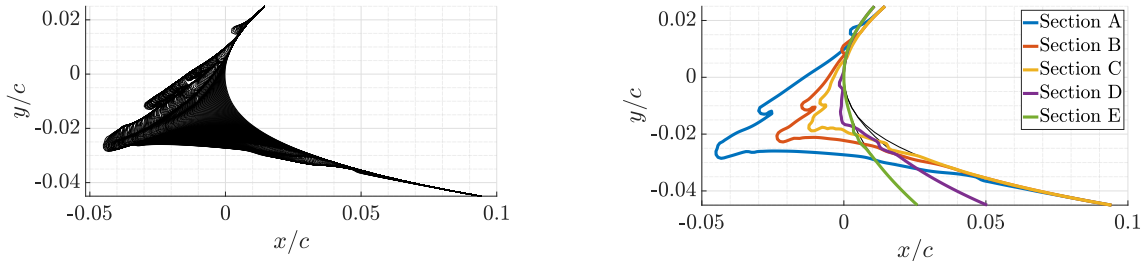

(a) Multi-step ice accretion on Section A

(b) Comparison of the ice shapes on sections A-E

Figure 4: Results of the ice accretion simulations.

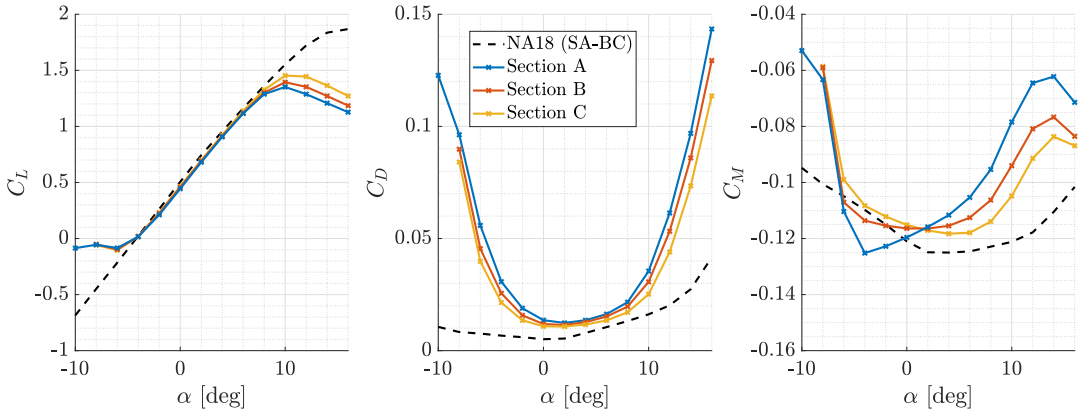

Figure 5: Aerodynamic coefficients of the iced sections with the NACA airfoil.

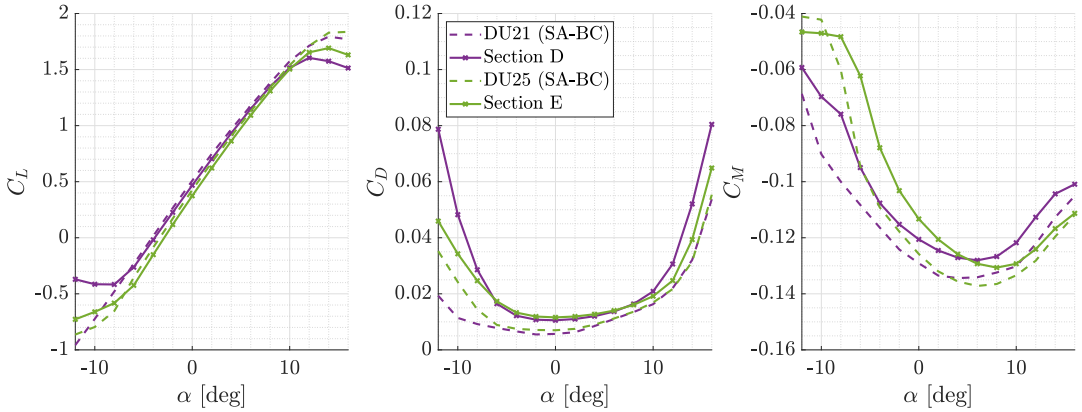

Figure 6: Aerodynamic coefficients of the iced sections with DU airfoils.

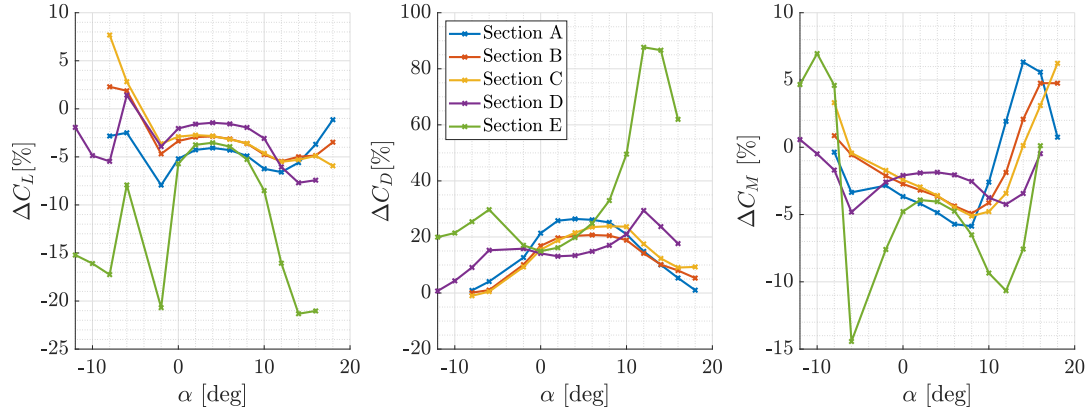

Figure 7: Effect of roughness extension on the aerodynamic coefficients of the different sections.

3.2 Estimation of Power Losses

The aeroelastic response of the wind turbine is now computed with OpenFAST with the different sets of data to produce power curves in turbulent wind, which are shown in Figure 8a. The IEC Kaiman spectral model for atmospheric turbulence is adopted. The reference solution considered for the clean configuration is the one obtained with SA-BC turbulence model, which provided an error smaller than 1% in extracted power if compared to NREL data above cut-in wind speed. Results are also compared with Etemaddar, who considered Mann [20] spectral model for atmospheric turbulence. In the considered operating conditions and accretion times, and with the imposed equivalent sand-grain roughness height, the effect of the extension of roughness has little effect on the power extracted from the wind turbine. In fact, ice shapes on the NACA sections are already well developed [21].

The percentage power loss, shown in Figure 8b, strongly depends on wind speed, as was found by Etemaddar. Results at cut-in wind speed are highly dependent on the random seed used to generate the realisation of the turbulent wind. The power loss decreases as the mean freestream wind speed increases, becoming lower than 1% at $13\,\mathrm{m\,s^{-1}}$, when the wind turbine starts to operate in Region 3 most of the time, regulating the pitch angle to reduce excesses in power production.

In Figure 8c the power coefficient (C_P) is shown as a function of the tip-speed ratio (TSR) for a pitch angle $\theta = 0°$, i.e., the pitch angle used before rated wind speed. The effect of the increased roughness on power coefficient is negligible at high TSR, while it is more evident for tip-speed ratios lower than the optimum one. Compared to the clean blade, the decrease in C_P is maximum at TSR values higher than the optimum one: in fact, the decrease in power output is maximum at low wind speeds, where the wind turbine operates at high TSR values. Thus, power losses at these wind speeds may be reduced by modifying the tabulated generator torque-speed relation to reach the rated tip-speed ratio at a lower generator speed, i.e. at a lower freestream wind speed.

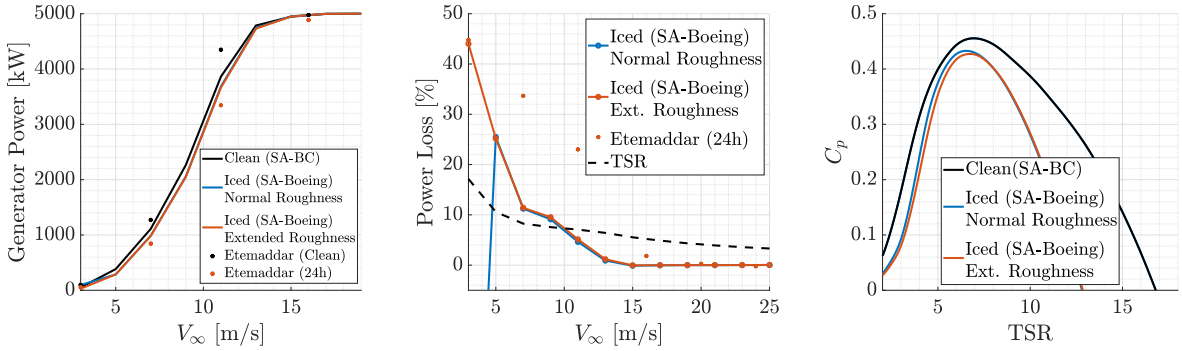

(a) Power Curves **(b)** Power Losses **(c)** C_P - TSR Curves

Figure 8: Wind turbine performance before and after icing.

4 CONCLUSIONS

High-fidelity ice accretion simulations were performed on a wind turbine blade, considering operation in a steady wind. To better represent the physics underlying the ice accretion process, a quasi-continuum approach was chosen for the multi-step simulations, providing both higher accuracy and a reduced computational effort. Ice geometry are finely discretised. After reproducing the aerodynamics of the clean blade, the aerodynamic coefficients of the iced sections were computed. The effect of surface roughness on the boundary layer was considered, assessing the effect of the extension of surface roughness in the icing event under analysis. Finally, the performances of the wind turbine were computed in a real scenario. Power losses are found to be highly dependent on the freestream wind speed, and, in fact, depend on TSR. A small influence of the extension of surface roughness was found. Finally, it was proposed to modify the tabulated generator torque-speed relation to reduce power losses at low wind speeds.

References

[1] M. C. Homola et al. "Performance losses due to ice accretion for a 5 MW wind turbine". In: *Wind Energy* 15.3 (2012), pp. 379–389.

[2] J. Jonkman et al. *Definition of a 5 MW reference wind turbine for offshore system development*. Tech. rep. NREL/TP-500-38060. National Renewable Energy Lab.(NREL), Golden, CO (United States), 2009.

[3] V. Turkia, S. Huttunen, and T. Wallenius. *Method for estimating wind turbine production losses due to icing*. VTT Technology 114. Project code: 72921. VTT Technical Research Centre of Finland, 2013.

[4] M. Etemaddar, M. O. L. Hansen, and T. Moan. "Wind turbine aerodynamic response under atmospheric icing conditions". In: *Wind Energy* 17.2 (2014), pp. 241–265.

[5] M. B. Bragg. "Rime ice accretion and its effect on airfoil performance". PhD thesis. The Ohio State University, 1982.

[6] A. Zanon, M. De Gennaro, and H. Kühnelt. "Wind energy harnessing of the NREL 5 MW reference wind turbine in icing conditions under different operational strategies". In: *Renewable Energy* 115 (2018), pp. 760–772.

[7] IEC 61400-1 Ed. 3. *Wind Turbines - Part 1: Design requirements*. International Electrotechnical Commission, 2005.

[8] F. Palacios et al. "Stanford University Unstructured (SU2): Analysis and Design Technology for Turbulent Flows". In: *52nd Aerospace Sciences Meeting*.

[9] *Main repository for the NREL-supported OpenFAST whole-turbine simulation code.* `https://web.archive.org/web/20201211063037/https://github.com/OpenFAST/openfast`. Accessed: 2020-12-11.

[10] T. Bellosta, G. Parma, and A. Guardone. "A robust 3D particle tracking solver for in-flight ice accretion using arbitrary precision arithmetic". In: *VIII International Conference on Computational Methods for Coupled Problems in Science and Engineering*. CIMNE. 2019, pp. 622–633.

[11] G. Gori et al. "PoliMIce: A simulation framework for three-dimensional ice accretion". In: *Applied Mathematics and Computation* 267 (2015), pp. 96–107.

[12] D. Dussin et al. "Hybrid grid generation for two-dimensional high-Reynolds flows". In: *Computers & fluids* 38.10 (2009), pp. 1863–1875.

[13] W. Wright. *User's manual for LEWICE version 3.2*. Tech. rep. CR-214255. NASA, 2008.

[14] V. Venkatakrishnan. "On the accuracy of limiters and convergence to steady state solutions". In: *31st Aerospace Sciences Meeting*. 1993, p. 880.

[15] I. B. Celik et al. "Procedure for estimation and reporting of uncertainty due to discretization in CFD applications". In: *Journal of fluids Engineering-Transactions of the ASME* 130.7 (2008).

[16] P. Spalart and S. Allmaras. "A one-equation turbulence model for aerodynamic flows". In: *30th aerospace sciences meeting and exhibit*. 1992, p. 439.

[17] S. C. Cakmakcioglu, O. Bas, and U. Kaynak. "A correlation-based algebraic transition model". In: *Proceedings of the Institution of Mechanical Engineers, Part C: Journal of Mechanical Engineering Science* 232.21 (2018), pp. 3915–3929.

[18] B. Aupoix and P. R. Spalart. "Extensions of the Spalart–Allmaras turbulence model to account for wall roughness". In: *International Journal of Heat and Fluid Flow* 24.4 (2003), pp. 454–462.

[19] Y. Han, J. Palacios, and S. Schmitz. "Scaled ice accretion experiments on a rotating wind turbine blade". In: *Journal of Wind Engineering and Industrial Aerodynamics* 109 (2012), pp. 55–67.

[20] J. Mann. "The spatial structure of neutral atmospheric surface-layer turbulence". In: *Journal of Fluid Mechanics* 273 (1994), pp. 141–168.

[21] L. Battisti. "Aerodynamic Performances of Ice Contaminated Rotors". In: *Wind Turbines in Cold Climates*. Springer, 2015, pp. 113–176.